




Finite-size effects in lead scandium tantalate relaxor thin filmsAbel Fernandez,¹ Jieun Kim ¹, Derek Meyers,^{1,*} Sahar Saremi,¹ and Lane W. Martin ^{1,2,†}¹*Department of Materials Science and Engineering, University of California, Berkeley, California 94720, USA*²*Materials Sciences Division, Lawrence Berkeley National Laboratory, Berkeley, California 94720, USA* (Received 21 November 2019; revised manuscript received 5 February 2020; accepted 19 February 2020; published 4 March 2020)

Large electromechanical effects in relaxor ferroelectrics are generally attributed to the collective response of an ensemble of correlated, nanometer-sized polar structures induced by chemical and charge disorder. Here, we study finite-size effects on such polar order (i.e., how it evolves when sample dimensions approach the polarization correlation length) in 7–70-nm-thick films of the relaxor ferroelectric $\text{PbSc}_{0.5}\text{Ta}_{0.5}\text{O}_3$. Temperature-dependent polarization studies reveal a linear suppression of the polarization and nonlinearity associated with relaxor order as the film thickness decreases to ≈ 30 nm. Below this thickness, however, the suppression rapidly accelerates, and polarization is completely absent by film thicknesses of ≈ 7 nm, despite the continued observation of a broad peak in dielectric permittivity and frequency dispersion. Diffuse-scattering measurements reveal the diffuse-scattering symmetry, and analysis suggests the films have a polarization correlation length of ≈ 23 nm. Taken together, it is apparent that reduction of sample size and the resulting distribution of polar structures drive suppression and eventual quenching of the electrical response of relaxors, which may be attributed to increasing dipole-dipole and dipole-interface interactions.

DOI: [10.1103/PhysRevB.101.094102](https://doi.org/10.1103/PhysRevB.101.094102)**I. INTRODUCTION**

Relaxor ferroelectrics are of great interest for their large electromechanical responses and are promising candidates for a variety of sensor, energy-harvesting, and energy storage applications [1–3]. Chemical and charge disorder in perovskite-based relaxors drives local symmetry breaking, reduces polar correlations to nanometer-sized regions, and introduces a complex polar evolution with temperature. The polar structure within relaxors has been described as a distribution of polar nanoregions embedded in a nonpolar matrix or polar nanodomains with low-angle domain walls [4–6]. While the explicit nature of these polar clusters remains the subject of ongoing investigation, the temperature evolution of the polar structure is widely recognized to exhibit four distinct critical points. First, the local polarization forms from the high-temperature paraelectric phase upon cooling through the Burns temperature T_b , below which the dynamically correlated polarization rapidly fluctuates due to thermal excitations [7]. As the temperature is further lowered, the local dynamic polarization becomes more strongly correlated, leading to the formation of static atomic displacements at an intermediate temperature T^* [8]. With further cooling, polar clusters grow and begin to impinge upon each other, increasing their relaxation time, thus giving rise to the observation of a frequency-dependent dielectric maximum temperature T_m . The frequency dependence of the dielectric maximum temperature can be described using the Vogel-Fulcher freezing

model, developed in both structural and magnetic-glass systems, where the progressive slowing down of relaxation times leads to the formation of a percolative network of the largest, slowest polar clusters at the freezing temperature T_f [9–11]. This evolution of the polar order with temperature and the stimuli-driven electromechanical response of relaxors more generally are highly dependent on the size and interaction of these polar clusters. As such, much effort has been focused on the characterization and manipulation of polar correlations in relaxors. While neutron and x-ray diffraction-based measurements of polar-disorder-induced diffuse scattering have been used to probe the length scales of polar interactions in macroscopic bulk and single-crystal samples, only recently have these techniques been applied to thin films [12–14].

Of fundamental importance to relaxor properties is the connection between local and long-range polar structure. Whereas the bistable, spontaneous polarization in normal ferroelectrics has its origin in atomic interactions at the unit-cell level [15], relaxor properties are derived from the mesoscopic interactions of an ensemble of polar entities with distinct anisotropies, magnitudes, and relaxation times. Thus, among a range of open questions, there remains interest in the effect of reducing sample dimensions to the length scale of polar interactions. While finite-size effects have been studied extensively in ferroelectrics (revealing the potential for robust polarization down to the level of just a few unit cells [16,17]), few studies, focusing mostly on grain-size-dependent effects in bulk ceramics, have explored similar concepts in relaxors [18–22]. Such studies face the additional challenge of having to alter the synthesis process to achieve different grain sizes, thus introducing variations in the degree of chemical order and disorder, grain-boundary density, and porosities, all of which can add to the complexity of studying these complex polar

*Present address: Department of Physics, Oklahoma State University, Stillwater, Oklahoma 74078, USA.

†lwmartin@berkeley.edu

interactions. Only in the last few years have advances in thin-film synthesis and commercially available substrates enabled the high-quality growth of these materials, thus opening up new pathways to study finite-size effects in relaxors [14].

Here, we study the role of finite-size effects on the evolution of relaxor order in epitaxial thin films of $\text{PbSc}_{0.5}\text{Ta}_{0.5}\text{O}_3$. While this composition and other relaxor materials have been extensively studied in the bulk, there is relatively little information on epitaxial thin films. Utilizing films from 7 to 70 nm thick, temperature- and electric-field-dependent dielectric and polarization studies reveal a general suppression of the polarization and a reduction in the nonlinearity typically associated with relaxor order in the thinnest films. This suppression scales linearly until a film thickness of ≈ 30 nm, at which point the suppression accelerates rapidly, and by a film thickness of ≈ 7 nm the nonlinearity is absent, despite the observation of a broad peak in dielectric permittivity and frequency dispersion. Diffuse-scattering measurements reveal the diffuse-scattering symmetry and a polarization correlation length of ≈ 23 nm, suggesting the change in scaling of polarization response is associated with a critical interaction of polar correlations and sample size. All told, rather than fundamentally changing the polar structure, the reduction of film thickness drives a suppression of collective polarization response, limiting the polarization response to that of the intrinsic lattice, which resembles that of a linear dielectric.

II. EXPERIMENT

Heterostructures of 80-nm SrRuO_3 /7-, 15-, 22-, 30-, 50-, and 70-nm $\text{PbSc}_{0.5}\text{Ta}_{0.5}\text{O}_3$ /30-nm SrRuO_3 /DyScO₃ (110) were synthesized via pulsed-laser deposition. The SrRuO_3 bottom electrodes were grown at a heater temperature of 690 °C in a dynamic oxygen pressure of 100 mTorr with a laser fluence of 1.3 J/cm² and a laser repetition rate of 15 Hz from a ceramic target of the same composition (Praxair). The $\text{PbSc}_{0.5}\text{Ta}_{0.5}\text{O}_3$ layers were grown at a heater temperature of 550 °C in a dynamic oxygen pressure of 200 mTorr with a laser fluence of 1.5 J/cm² and a laser repetition rate of 2 Hz from a ceramic target of the same composition with 10% lead excess to compensate for lead loss during growth. The SrRuO_3 top electrode layers were grown *in situ* immediately following $\text{PbSc}_{0.5}\text{Ta}_{0.5}\text{O}_3$ deposition using the same laser and pressure conditions used for the SrRuO_3 bottom electrode, at a reduced heater temperature of 550 °C to prevent volatilization of lead from the underlying $\text{PbSc}_{0.5}\text{Ta}_{0.5}\text{O}_3$ layer during growth. Following deposition, the heterostructures were cooled at a rate of 10 °C/min in a static oxygen pressure of 760 Torr.

Structural characterization was completed using x-ray θ - 2θ line scans and two-dimensional (2D) reciprocal space mapping (RSM) studies which were conducted with a high-resolution x-ray diffractometer (X'pert³ MRD, PANalytical). Further synchrotron x-ray three-dimensional (3D) reciprocal space mapping studies, particularly focused on the extraction of diffuse-scattering patterns, were conducted using a Huber 4-circle diffractometer and Pilatus 100K pixel detector with x-ray energy of 16 keV at beamline 33-BM-C at the Advanced Photon Source, Argonne National Laboratory. Chemical analysis of the films was accomplished using Rutherford backscattering spectrometry (RBS, incident ion energy of

3040 keV, incident angle $\alpha = 22.5^\circ$, exit angle $\beta = 25.35^\circ$, and scattering angle $\theta = 168^\circ$), and the spectra were fit using the RBS analysis software SIMNRA [23].

Electrical measurements were performed on circular capacitor structures of $\text{PbSc}_{0.5}\text{Ta}_{0.5}\text{O}_3$ with symmetric SrRuO_3 electrodes. The top electrodes were defined using a photoresist mask and subsequent SrRuO_3 -selective wet etching utilizing sodium metaperiodate (NaIO_4). Capacitors with diameters of 32, 25, 16, and 12.5 μm were measured with no appreciable difference observed between measurements on different capacitor sizes. Temperature-dependent dielectric permittivity measurements, permittivity-DC bias sweeps, and nonlinearity studies were performed using an impedance analyzer (E4990A, Keysight Technologies). The temperature-dependent dielectric permittivity was measured from 83 to 553 K using a cryogenic vacuum probe-station (TTPX, Lake Shore Cryotronics Inc.) by driving the top electrode with an AC voltage of 5 mV from 1 to 100 kHz. DC bias sweeps were measured by driving the top electrode with an AC voltage of 5 mV at 10 kHz while the DC bias was swept from ± 1000 kV/cm. AC field-dependent permittivity studies were measured by sweeping the AC voltage applied to the top electrode. The harmonic analysis was performed using a wave form generator to apply an AC voltage to the top electrode and collect current from the bottom electrode through a lock-in amplifier (SRS 830, Stanford Research Systems) to measure the phase angle between the first and third harmonics of polarization. Polarization-electric-field hysteresis loops were measured at a frequency of 10 kHz using a Precision Multi-ferroic Tester (Radiant Technologies).

III. RESULTS AND DISCUSSION

RBS studies reveal that, in all cases, the films are stoichiometric to the expected chemistry within the error of the measurement (Supplemental Material, Fig. S1 [24]). X-ray diffraction studies (Supplemental Material, Fig. S2 [24]) reveal the production of single-phase, 00 l -oriented $\text{PbSc}_{0.5}\text{Ta}_{0.5}\text{O}_3$ films and that the out-of-plane lattice parameter for all films, regardless of thickness, was 4.075 ± 0.03 Å [Fig. 1(a)]. This agrees with bulk studies [25] and is consistent with the production of fully relaxed films (as is expected based on the large -3.3% lattice mismatch between $\text{PbSc}_{0.5}\text{Ta}_{0.5}\text{O}_3$ and DyScO₃). Subsequent RSM studies of the 103 and 332 diffraction conditions of $\text{PbSc}_{0.5}\text{Ta}_{0.5}\text{O}_3$ and DyScO₃, respectively, confirm this observation (Supplemental Material, Fig. S3 [24]). Analysis of the x-ray rocking curves reveals that, despite the relaxed nature of the films, a high degree of crystallinity is maintained, as demonstrated by the full width at half maximum of $\approx 0.04^\circ$ of the 002 diffraction peak of $\text{PbSc}_{0.5}\text{Ta}_{0.5}\text{O}_3$ compared to that of $\approx 0.006^\circ$ for the DyScO₃ substrate (Supplemental Material, Fig. S4). All told, the set of films studied herein has equivalent structures, strain states, and crystallinity, thus providing a model set of materials to explore finite-size effects on polar-order evolution in relaxor ferroelectrics.

In order to understand the effect of changing thickness on the temperature evolution of polar order, temperature-dependent, low-field dielectric permittivity [Fig. 1(b)], and loss (Supplemental Material, Fig. S5 [24]) studies were

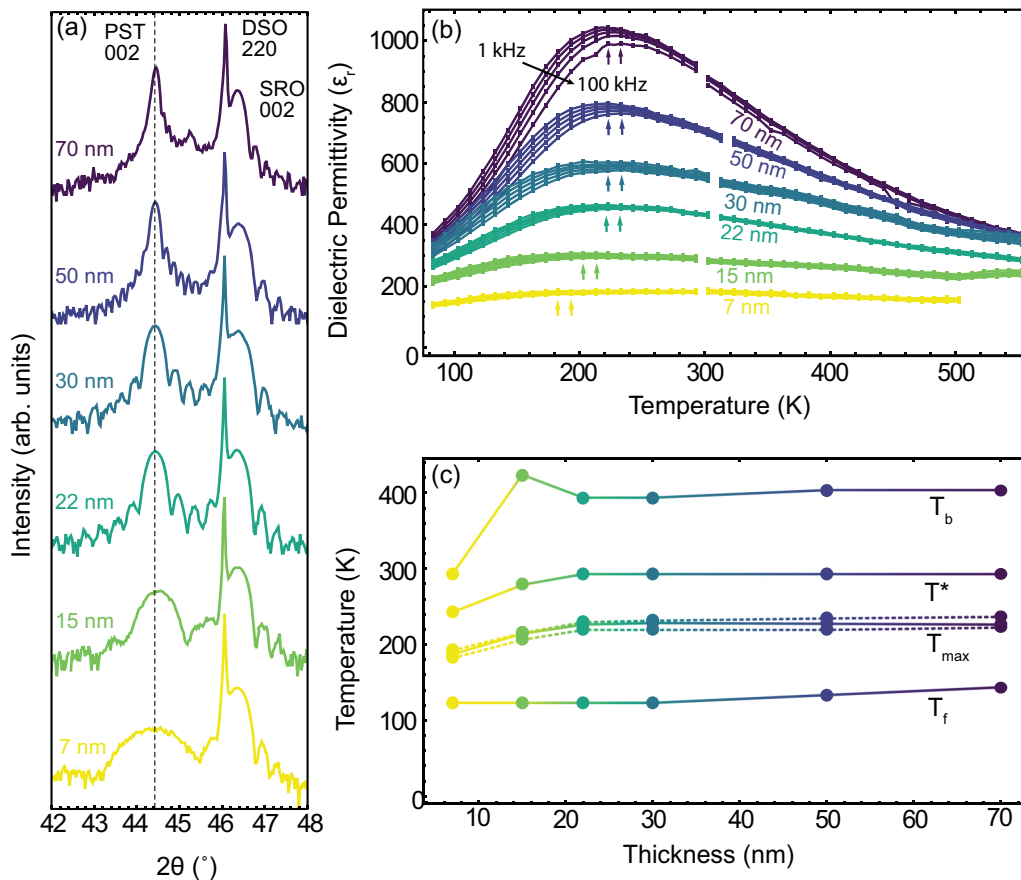


FIG. 1. (a) X-ray diffraction θ - 2θ scans of the $\text{PbSc}_{0.5}\text{Ta}_{0.5}\text{O}_3/\text{SrRuO}_3/\text{DyScO}_3$ heterostructures indicate the bulklike lattice parameter of $\text{PbSc}_{0.5}\text{Ta}_{0.5}\text{O}_3$ is maintained in all thicknesses studied. (b) Temperature-dependent dielectric permittivity studies show the suppression of permittivity at reduced thickness. T_m (marked with arrows for 1 and 100 kHz) changes only below 22 nm. (c) The four critical temperatures are summarized as a function of thickness.

completed and used to extract T_b , T_m , T^* , and T_f (Supplemental Material, Fig. S6). The overall magnitude of the dielectric permittivity is found to systematically reduce with decreasing film thickness, with the maximum permittivity changing from ≈ 1000 in the 70-nm-thick films to just ≈ 200 in the 7-nm-thick films. Despite this change, all films reveal broad temperature evolution and frequency dispersion of the dielectric response (between 1 and 100 kHz the change in T_m is ≈ 10 K) which agrees with bulk data, thus suggesting that the films have a similar degree of relaxor character [26–28]. T_m is found to be ≈ 40 K lower than typical bulk samples; however, similar shifts have been observed in bulk samples depending on synthesis conditions and in sol-gel-derived films [29–32]. A summary of the various critical temperatures, as a function of film thickness, is provided [Fig. 1(c)]. Starting from the thickest films, a negligible change is observed for T_b , T_m , and T^* , while T_f decreases slightly as the thickness is reduced to 30 nm. Upon transitioning to thicknesses ≤ 22 nm, however, significant changes in the critical temperatures are seen. First, T_b undergoes negligible changes down to film thicknesses of ≈ 15 nm, at which point a slight increase is observed, before a large decrease occurs in the thinnest (7 nm) films. T_m and T^* both decrease in the thinnest films, but T_f remains essentially constant at ≈ 120 K in the thin-film regime. The shifting of the various temperatures follows an interesting

trend with thickness; whereas T_b changes significantly only in the thinnest films (7 and 15 nm), T_f is already decreasing in 50-nm-thick films. Because T_f is associated with the percolative freezing of the largest and slowest polar clusters [9], it is possible that finite-size effects appear at larger thickness, while T_b is related to the nucleation of highly local polarization and therefore is influenced only in the thinnest films [6]. The general picture presented by the temperature evolution is that the polar structures and their temperature evolution are relatively unaffected by film thickness until the films pass into a thickness regime ≤ 22 nm. Another interesting observation, however, is that the maximum of the dielectric permittivity has a strong dependence on film thickness even at the largest thicknesses studied, indicating a strong influence of sample size on relaxor response. We note that at temperatures above T_b and below T_f , where polar clusters are dissolved into a paraelectric phase or frozen and unable to respond, respectively, the dielectric permittivity of the thickest films (≥ 30 nm) approaches the same value of ≈ 300 , suggesting the dominant difference between films of different thickness is the extrinsic response and interaction of polar clusters rather than the intrinsic lattice response of the material [33].

To better understand the role of intrinsic and extrinsic polarization response in these films, the dielectric permittivity

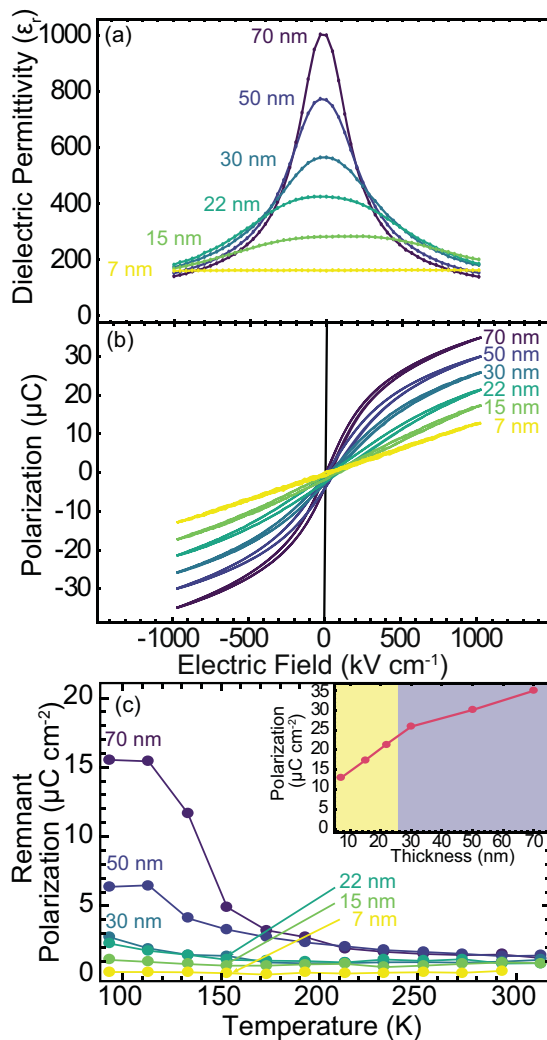


FIG. 2. (a) Dielectric tunability and (b) polarization-electric-field hysteresis loops show a suppression of dielectric and polarization response with decreasing thickness, indicating a suppression of extrinsic contributions. (c) Temperature dependence of the remnant polarization shows that thicker films have larger remanence at all thicknesses and the thinnest films never develop strong remanence even at low temperature. Inset: Scaling of the maximum polarization as a function of thickness shows a distinct change in scaling below 30 nm.

was measured as a function of DC bias [Fig. 2(a)]. The effect of the DC bias is to reorient the polar structures, thus suppressing extrinsic contributions and reducing the overall permittivity [34]. We observe the characteristic large tunability expected of relaxors in thicker films (i.e., >30 nm), but the tunability is continually reduced with decreasing thickness until the tunability is completely suppressed in the 7-nm-thick films. At large DC bias fields, the permittivity of all films approaches ≈ 200 , supporting the hypothesis that the intrinsic dielectric permittivity of the films is relatively unchanged by the reduced thickness. Instead, the primary difference between the different thicknesses is observed at low DC bias fields, where extrinsic contributions are active. Further insight is garnered from polarization-electric-field loops [Fig. 2(b)], where a similar trend of reduced polarization response

and suppressed nonlinearity with decreasing thickness are observed. In fact, the 7-nm-thick films behave like linear dielectrics, with no nonlinearity even under applied fields of 1 MV/cm. It is also worth noting that, despite reports of stabilization of polar clusters into ferroelectric domains in ultrathin films, no change in remnant polarization is observed with film thickness, suggesting that the stabilization of ferroelectricity at reduced dimensions seems unlikely [35]. Moreover, this behavior is maintained throughout the temperature range studied, with the increase in remnant polarization at low temperatures becoming more pronounced for thicker films, rather than thinner films; again the 7-nm-thick films never develop nonlinearity or hysteresis [Fig. 2(c)]. In addition to suppressed dielectric permittivity, we also note that the curvature of the hysteresis loops at high fields (≈ 400 – 800 kV/cm), which is associated with the nonlinear response of reorienting polar clusters [36], is also suppressed with decreasing thickness. Together, these observations suggest that reduction of sample dimensions suppresses the nonlinear, extrinsic contributions from mobile polar clusters, essentially stiffening the relaxor response until only the intrinsic response is observed in 7-nm-thick films. Notably, the suppression of field-induced polarization appears to be linear with decreasing thickness, with a distinct change in slope between 20 and 30 nm [Fig. 2(c), inset].

Considering the observation of suppressed nonlinearity at reduced thickness, we explored additional ways to quantify the changes in nonlinearity and dielectric response as a function of applied AC field. Nonlinearity in ferroelectrics has been studied within the context of Rayleigh-type domain-wall motion in a random distribution of pinning sites, where measurement of the AC-field dependence reveals regimes of reversible and irreversible (or hysteretic) contributions [37]. Under the application of small AC fields, domain walls oscillate within their potential well, unable to overcome the energy barrier of the local pinning site, and the dielectric response remains flat. As the field is increased, the driving force becomes strong enough to drive domain walls over the energy barrier, allowing them to contribute to the dielectric response. The dielectric permittivity of the $\text{PbSc}_{0.5}\text{Ta}_{0.5}\text{O}_3$ films was measured as a function of applied AC field at 353 K [Fig. 3(a)], 253 K [Fig. 3(b)], 153 K [Fig. 3(c)], and 93 K [Fig. 3(d)], revealing a strong dependence of nonlinearity on film thickness and temperature. The data presented have been normalized to the low-field permittivity to better visualize the change in permittivity with increasing applied field. With the exception of the 7-nm-thick films, all thicknesses show qualitatively similar behavior. At 353 K [Fig. 3(a); above T^*], the permittivity decreases with increasing field, in agreement with the thermally activated nature of the fluctuating polar dipoles between T^* and T_b . Lowering the temperature below T^* brings the appearance of a peak in the permittivity with increasing field, revealing the transition to domain-type dynamics owing to the static off centering of cations [38]. This static off centering comes about owing to development of a local potential well, and the increase in permittivity with increasing field appears similar to that expected for normal ferroelectrics. At even larger fields, however, a maximum in the permittivity appears, indicating that the majority of clusters are responding to the applied field. Beyond these AC

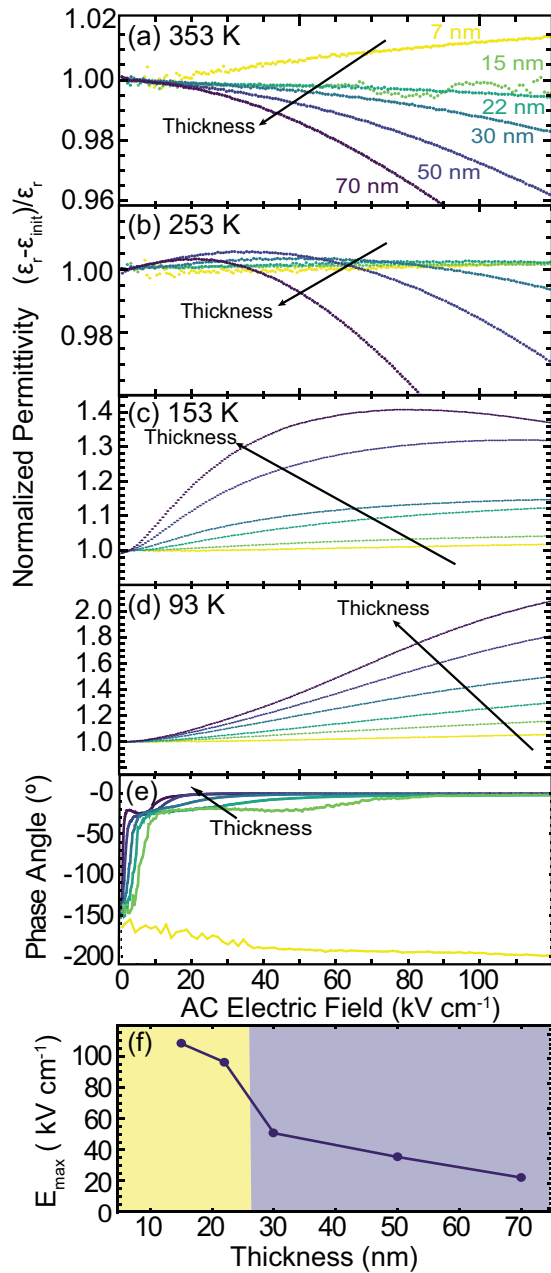


FIG. 3. Nonlinearity studies performed at (a) 353 K, (b) 253 K, (c) 153 K, and (d) 93 K show the evolution of dielectric response to the AC field, indicating the onset of domain-type dynamics below T^* and the progressive slowing down and freezing of polar structures below T_m . (e) The phase angle of the third harmonic measured at 253 K shows the progressive increase in field required to maximize dielectric response. (f) The trend in E_{max} as a function of thickness shows a distinct change in scaling below 30 nm, similar to the polarization scaling.

fields, the permittivity decreases, an effect that was previously attributed to either reorientation and saturation of polar-cluster response or tunability of the permittivity, akin to DC bias measurements [39]. As the temperature is further lowered, the low-field permittivity is suppressed, but the degree to which increasing field can activate more regions increases from a few percent at 253 K [Fig. 3(b)] to 40% at 153 K [Fig. 3(c)] and

100% at 93 K [Fig. 3(d)] in the 70-nm-thick films. This trend can be understood in the context of the energy landscape for polar displacements in relaxors, where local potential wells become deeper with decreasing temperature, requiring larger fields to drive dielectric response. In conjunction with DC bias and polarization measurements, measurements of nonlinear dielectric response discussed here indicate that reducing film thickness suppresses the ability of polar structures to respond to applied electric fields, until the ability to respond is completely quenched in 7-nm films.

In addition to the dielectric permittivity, measurement of higher-order harmonics of the permittivity provide additional insight into the dynamic motion of polarization contributions [40], and specifically, the phase angle δ_3 between the first and third harmonics has been used to quantify the onset of the hysteretic response of ferroelectric domain-wall motion. In ferroelectrics, the low-field reversible regime is marked by a δ_3 which remains $\approx -180^\circ$. At larger fields, depinning of domain walls appears as a rapid increase of δ_3 to $\approx -90^\circ$, where it plateaus as domain walls are hysteretically moved with the oscillating field. In contrast, the highly reversible and anhysteretic response of relaxors imparts quantitatively distinct behavior, as shown in $\text{PbMg}_{1/3}\text{Nb}_{2/3}\text{O}_3$ ceramics, where δ_3 changes from $\approx -180^\circ$ at low fields to $\approx 0^\circ$ at higher fields [39]. δ_3 was measured at 253 K to understand the origin and thickness dependence of the peak that appears in the permittivity below T^* . All films exhibit an increase in δ_3 from $\approx -160^\circ$ to $\approx 0^\circ$ [Fig. 3(e)], with the exception of the 7-nm-thick films, which show minimal changes with field, as expected for a dielectric [39]. The field at which $\delta_3 \approx 0^\circ$, corresponding to the field at which the permittivity is maximized E_{max} , appears to increase with decreasing thickness. The presence of an intermediate plateau $\delta_3 \approx -25^\circ$ also reveals large differences between films of different thicknesses. While the origin of this intermediate phase angle is not well understood, it may be due to a convolution of contributions from both hysteretic ($\delta_3 \approx -90^\circ$) and anhysteretic ($\delta_3 \approx 0^\circ$) motion of polar structures, whose combined polarization response has an intermediate-phase offset. In this case, the proportion of hysteretic contributors appears to be unchanged by film thickness, as the plateau occurs at the same δ_3 for all films, but decreasing thickness changes the depth of the local wells, necessitating larger fields to drive the maximum dielectric response. By analogy to the effect of reducing temperature, the effect of decreasing film thickness appears to be similar to that of the deepening of local potential wells, suppressing the total polarization response that can be achieved and increasing the field needed to drive polarization response.

To visualize this, we examine E_{max} as a function of thickness [Fig. 3(f)]. A linear increase in E_{max} is observed for films from 70 to 30 nm thick; however, a sharp increase in E_{max} occurs below 30 nm [Fig. 3(f)], similar to the behavior observed for scaling of the polarization [Fig. 2(c), inset]. The linear decrease at large thicknesses indicates a proportional scaling of electrical response with thickness, suggesting the interaction of polar clusters is directly related to the length scale over which they can interact. This type of behavior has been suggested in efforts to model dipolar interactions in relaxors, where the energy associated with interacting dipoles

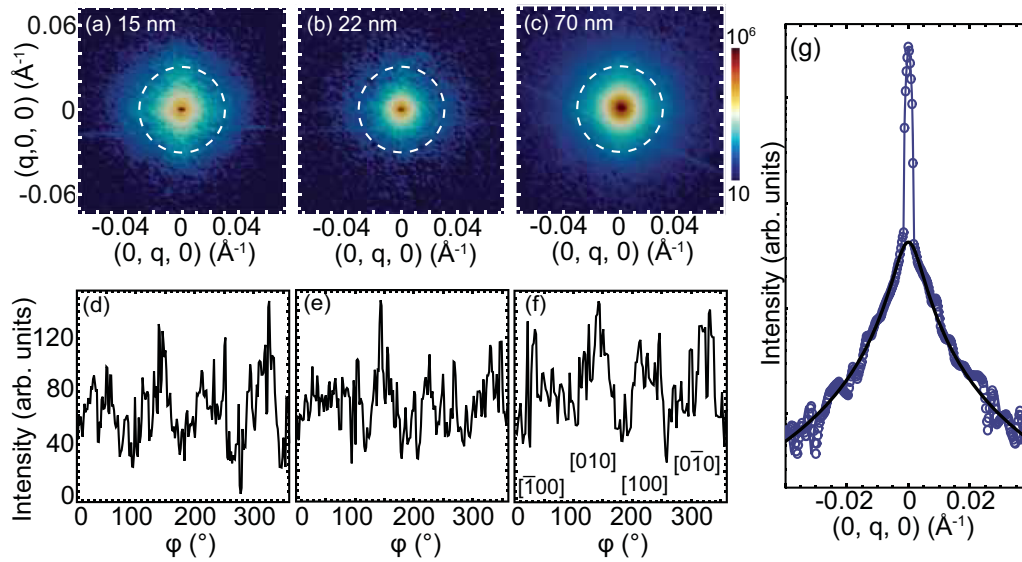


FIG. 4. Two-dimensional intensity plots of 3D RSM studies performed at 153 K to observe diffuse scattering from polar distortions. (a) The 15-nm, (b) 22-nm, and (c) 70-nm films show a clover-shaped diffuse scattering pattern that is visualized by taking a radial line cut at $q = 0.027 \text{ \AA}^{-1}$ (white dashed line), showing the intensity variation from the four lobes. (d)–(f) The intensity variation along the radial line cut shows four lobes of intensity with crystallographic directions labeled in (f). (g) Correlation-length analysis is performed on 15-nm films by taking a line cut along the [100] direction and fitting to Eq. (1) (black line), resulting in a polar correlation length of 23 nm.

in high-permittivity crystals was shown to be inversely proportional to the volume of the crystal [41,42]. While this effect may play a relatively minor role in macroscopic samples, reduction of the crystal volume to sizes more comparable to the dipole correlation length may lead to the strong thickness dependence observed here. The change in scaling observed below 30 nm, however, necessitates further study.

The strong dependence of relaxor behavior on the distribution of polar-cluster size and their interactions suggests the possibility of a fundamental change in properties when the sample size approaches the polarization correlation length. As such, understanding the polar structure and polarization correlation length is necessary to understand the change in scaling at reduced thickness. Diffuse-scattering measurements on $\text{PbMg}_{1/3}\text{Nb}_{2/3}\text{O}_3$, $\text{PbZn}_{1/3}\text{Nb}_{2/3}\text{O}_3$, and related relaxor materials have shown correlation lengths between 2 and 20 nm depending on chemistry and temperature [13,43]. The strong interplay between cluster size, relaxation time, and the critical temperatures associated with polar evolution in relaxors suggests that the consistency in critical temperatures for films of thicknesses ≥ 30 nm is a result of the polar structure remaining unaffected in this thickness regime. The changes to the response in films thinner than 30 nm, however, indicate a change in polar interactions. To understand the origin of this change, we performed three-dimensional RSM studies at 153 K to study the diffuse scattering from polar structures and determine the polar correlation length. Diffuse scattering was studied in 15-nm-thick [Fig. 4(a)], 22-nm-thick [Fig. 4(b)], and 70-nm-thick [Fig. 4(c)] films, and two-dimensional intensity maps of a slice through $(hk0)$ of the 002-diffraction condition for $\text{PbSc}_{0.5}\text{Ta}_{0.5}\text{O}_3$ show a clover-shaped diffuse-scattering pattern in all films studied, with diffuse intensity extending along [100], $[\bar{1}00]$, [010], and $[0\bar{1}0]$. The fourfold symmetry of the diffuse intensity is illustrated by a radial line cut [white dashed line in Figs. 4(a)–4(c)], graphed in

Figs. 4(d)–4(f)], showing four broad peaks separated by $\approx 90^\circ$. The symmetry of the diffuse intensity suggests a preferred direction for polar displacements, although further measurements, including measurements near other diffraction conditions, are required to fully describe the shape and orientation of polar regions [43]. While similar diffuse-scattering patterns are observed in all films studied, quantitative analysis of measurements from 22- and 70-nm-thick films is difficult owing to the presence of additional defect-scattering effects that overlaps with the cross-shaped pattern (further discussion on this matter is presented in the Supplemental Material, Fig. S8 [24]). Using these data, it is possible to perform correlation length analysis [13] on the data from the 15-nm-thick films by fitting the diffuse intensity to a Lorentzian profile [Fig. 4(g)]:

$$I_{diff} = \frac{I_0 \Gamma}{\pi(\Gamma^2 + q^2)}, \quad (1)$$

where Γ is the half width at half maximum, q is the distance from the center of the peak, and I_0 is the integrated intensity of the diffuse scattering. Taking the reciprocal of Γ provides a measure of the correlation length ξ of the polar structures, which was found to be ≈ 23 nm for these films. This coincides closely with the length scale at which the polarization scaling abruptly changes (≈ 30 nm), suggesting that this change is associated with an interaction of the thickness of the film with the average correlation length of the polar structures.

In light of this observation, we return to discussing the scaling behavior of the critical temperatures and polarization response of the films now in the context of this observation. Whereas the linear decrease in polarization response with decreasing thickness may be due to increasing dipolar interaction strength as the crystal volume is reduced, the change in scaling that occurs below 30 nm may be due to a critical interaction of the polar structures with the film interfaces. At the relaxor-electrode interfaces (both the top and bottom of

the film), weak depolarization fields arising from imperfect screening from the oxide electrodes can create interfacial regions where the small polar clusters are pinned into random orientations to reduce this depolarization field akin to the formation of 180° domains in ultrathin ferroelectrics [16,17,44]. As such, the observation that T_f begins decreasing at the largest thicknesses is likely evidence of the presence of larger clusters that begin interacting with the film thickness even at a film thickness of 50 nm. As thickness is further decreased to the length scale of polar correlations, it becomes increasingly likely that polar clusters may extend through the thickness of the film. This scenario has been proposed as a driving force for stabilization of ferroelectricity; however, the highly polarizable relaxor polar structures may allow for an internal compensation of depolarizing fields, increasing the interaction between adjacent dipoles in the lattice and accelerating the suppression of polarization response with decreasing thickness. This may also provide an explanation for the lack of non-linearity observed in the 7-nm-thick films, despite dielectric measurements showing a peak and frequency dispersion, since the film has not become purely dielectric, but only the smallest polar clusters and boundaries are still free to move, while most of the polarization is locked in strong locally anisotropic potential wells. Overall, the effect of reducing sample size (or thickness here) appears to be that of reducing the collective response of polar structures, limiting the polarization response to the intrinsic lattice response. The present results indicate that large electrical response in relaxors is highly dependent on the motion of the entire ensemble of polar clusters and is lost when the volume over which clusters can interact and reorient is restricted.

In summary, high-quality $\text{PbSc}_{0.5}\text{Ta}_{0.5}\text{O}_3$ thin films of varying thickness were synthesized and studied to understand

finite-size effects in relaxors. The temperature evolution of polar structure in the films is relatively insensitive to finite-size effects, with only small changes apparent below ≈ 22 nm, whereas the magnitude of the polarization response is continually suppressed with decreasing thickness. Between 20 and 30 nm, a distinct change in scaling is observed that is reflected in changes in the ability of the material to respond to applied fields. Structural characterization suggests this change in scaling behavior occurs when the film thickness approaches the average correlation length of the polar structures; however, considerably more study of the diffuse-scattering patterns is required. Ultimately, these results have important implications for understanding relaxor material response—both in small-grain-size ceramics and thin-film devices as the large electrical response typically associated with relaxors is greatly suppressed at reduced dimensions, placing a lower bound on the length scale at which relaxors can be utilized.

ACKNOWLEDGMENTS

A.F. acknowledges support from the National Science Foundation under Grant No. DMR-1708615. J.K. acknowledges support from the Army Research Office under Grant No. W911NF-14-1-0104. D.M. acknowledges support from the U.S. Department of Energy, Office of Science, Office of Basic Energy Sciences, Materials Sciences and Engineering Division under Contract No. DE-AC02-05-CH11231 (Materials Project program KC23MP) for the development of functional complex oxides. S.S. acknowledges support from the U.S. Department of Energy, Office of Science, Office of Basic Energy Sciences, under Award No, DE-SC-0012375 for the development of ferroic thin films. L.W.M. acknowledges support from Intel Corp. under the FEINMAN program.

-
- [1] F. Li, M. J. Cabral, B. Xu, Z. Cheng, E. C. Dickey, J. M. LeBeau, J. Wang, J. Luo, S. Taylor, W. Hackenberger, L. Bellaiche, Z. Xu, L.-Q. Chen, T. R. Shrout, and S. Zhang, *Science* **364**, 264 (2019).
 - [2] H. Pan, F. Li, Y. Liu, Q. Zhang, M. Wang, S. Lan, Y. Zheng, J. Ma, L. Gu, Y. Shen, P. Yu, S. Zhang, L.-Q. Chen, Y.-H. Lin, and C.-W. Nan, *Science* **365**, 578 (2019).
 - [3] S. Pandya, J. Wilbur, J. Kim, R. Gao, A. Dasgupta, C. Dames, and L. W. Martin, *Nat. Mater.* **17**, 432 (2018).
 - [4] L. E. Cross, *Ferroelectrics* **151**, 305 (1994).
 - [5] H. Takenaka, I. Grinberg, S. Liu, and A. M. Rappe, *Nature (London)* **546**, 391 (2017).
 - [6] J. Toulouse, *Ferroelectrics* **369**, 203 (2008).
 - [7] G. Burns and F. H. Dacol, *Jpn. J. Appl. Phys.* **24**, 85 (1985).
 - [8] B. Dkhil, P. Gemeiner, A. Al-Barakaty, L. Bellaiche, E. Dul'kin, E. Mojaev, and M. Roth, *Phys. Rev. B* **80**, 064103 (2009).
 - [9] R. Pirc and R. Blinc, *Phys. Rev. B* **76**, 020101(R) (2007).
 - [10] A. K. Tagantsev, *Phys. Rev. Lett.* **72**, 1100 (1994).
 - [11] D. Viehland, S. J. Jang, L. E. Cross, and M. Wuttig, *J. Appl. Phys.* **68**, 2916 (1990).
 - [12] D. La-Orautapong, J. Toulouse, J. L. Robertson, and Z.-G. Ye, *Phys. Rev. B* **64**, 212101 (2001).
 - [13] G. Xu, G. Shirane, J. R. D. Copley, and P. M. Gehring, *Phys. Rev. B* **69**, 064112 (2004).
 - [14] J. Kim, H. Takenaka, Y. Qi, A. R. Damodaran, A. Fernandez, R. Gao, M. R. McCarter, S. Saremi, L. Chung, A. M. Rappe, and L. W. Martin, *Adv. Mater.* **31**, 1901060 (2019).
 - [15] R. E. Cohen, *Nature (London)* **358**, 136 (1992).
 - [16] D. D. Fong, G. B. Stephenson, S. K. Streiffer, J. A. Eastman, O. Auciello, P. H. Fuoss, and C. Thompson, *Science* **304**, 1650 (2004).
 - [17] J. Junquera and P. Ghosez, *Nature (London)* **422**, 506 (2003).
 - [18] J. Carreaud, P. Gemeiner, J. M. Kiat, B. Dkhil, C. Bogicevic, T. Rojac, and B. Malic, *Phys. Rev. B* **72**, 174115 (2005).
 - [19] Y. Park, K. M. Knowles, and K. Cho, *J. Appl. Phys.* **83**, 5702 (1998).
 - [20] Q. Tan and D. Viehland, *Ferroelectrics* **193**, 157 (1997).
 - [21] C. Randall, A. Hilton, D. Barber, and T. Shrout, *J. Mater. Res.* **8**, 880 (1993).
 - [22] P. Papet, J. P. Dougherty, and T. R. Shrout, *J. Mater. Res.* **5**, 2902 (1990).
 - [23] SIMNRA, simnra.com.
 - [24] See Supplemental Material, which includes Refs. [45–53], at <http://link.aps.org/supplemental/10.1103/PhysRevB.101.094102> for additional characterization of the films used in

- this study, including Rutherford backscattering spectrometry, additional x-ray diffraction, and electrical characterization.
- [25] C. Caranoni, P. Lampin, and C. Boulesteix, *Powder Diffr.* **8**, 191 (1993).
- [26] N. Setter and L. E. Cross, *J. Appl. Phys.* **51**, 4356 (1980).
- [27] N. Setter and L. E. Cross, *J. Mater. Sci.* **15**, 2478 (1980).
- [28] I. Grinberg, P. Juhás, P. K. Davies, and A. M. Rappe, *Phys. Rev. Lett.* **99**, 267603 (2007).
- [29] F. Chu, N. Setter, and A. K. Tagantsev, *J. Appl. Phys.* **74**, 5129 (1993).
- [30] C. Malibert, B. Dkhil, J. M. Kiat, D. Durand, J. F. Bérar, and A. S.-d. Biré, *J. Phys.: Condens. Matter* **9**, 7485 (1997).
- [31] K. Brinkman, Y. Wang, M. Cantoni, D. Su, N. Setter, and P. Petrov, *J. Mater. Res.* **22**, 217 (2007).
- [32] K. Brinkman, A. Tagantsev, V. Sherman, D. Su, and N. Setter, *Phys. Rev. B* **73**, 214112 (2006).
- [33] F. Li, S. Zhang, T. Yang, Z. Xu, N. Zhang, G. Liu, J. Wang, J. Wang, Z. Cheng, Z.-G. Ye, J. Luo, T. R. ShROUT, and L.-Q. Chen, *Nat. Commun.* **7**, 13807 (2016).
- [34] A. K. Tagantsev and A. E. Glazounov, *Phys. Rev. B* **57**, 18 (1998).
- [35] D. Lee, H. Lu, Y. Gu, S.-Y. Choi, S.-D. Li, S. Ryu, T. R. Paudel, K. Song, E. Mikheev, S. Lee, S. Stemmer, D. A. Tenne, S. H. Oh, E. Y. Tsymbal, X. Wu, L.-Q. Chen, A. Gruverman, and C. B. Eom, *Science* **349**, 1314 (2015).
- [36] H. Fu and R. E. Cohen, *Nature (London)* **403**, 281 (2000).
- [37] D. Damjanovic and M. Demartin, *J. Phys. D* **29**, 2057 (1996).
- [38] A. E. Glazounov, A. K. Tagantsev, and A. J. Bell, *Phys. Rev. B* **53**, 11281 (1996).
- [39] S. Hashemizadeh and D. Damjanovic, *Appl. Phys. Lett.* **110**, 192905 (2017).
- [40] D. Damjanovic and D. V. Taylor, *Ferroelectrics* **221**, 137 (1999).
- [41] B. E. Vugmeister and H. Rabitz, *Phys. Rev. B* **57**, 7581 (1998).
- [42] B. E. Vugmeister and M. D. Glinchuk, *Rev. Mod. Phys.* **62**, 993 (1990).
- [43] G. Xu, Z. Zhong, Y. Bing, Z.-G. Ye, and G. Shirane, *Nat. Mater.* **5**, 134 (2006).
- [44] V. Nagarajan, J. Junquera, J. Q. He, C. L. Jia, R. Waser, K. Lee, Y. K. Kim, S. Baik, T. Zhao, R. Ramesh, P. Ghosez, and K. M. Rabe, *J. Appl. Phys.* **100**, 051609 (2006).
- [45] L. R. Dedon, S. Saremi, Z. Chen, A. R. Damodaran, B. Apgar, R. Gao, and L. W. Martin, *Chem. Mater.* **28**, 5952 (2016).
- [46] R. Gao, S. E. Reyes-Lillo, R. Xu, A. Dasgupta, Y. Dong, L. R. Dedon, J. Kim, S. Saremi, Z. Chen, C. R. Serrao, H. Zhou, J. B. Neaton, and L. W. Martin, *Chem. Mater.* **29**, 6544 (2017).
- [47] D. Viehland, S. Jang, L. E. Cross, and M. Wuttig, *Philos. Mag. B* **64**, 335 (1991).
- [48] P. H. Dederichs, *Phys. Rev. B* **4**, 1041 (1971).
- [49] P. H. Dederichs, *J. Phys. F* **3**, 471 (1973).
- [50] B. Dkhil, J. M. Kiat, G. Calvarin, G. Baldinozzi, S. B. Vakhrušev, and E. Suard, *Phys. Rev. B* **65**, 024104 (2001).
- [51] G. Xu, J. Wen, C. Stock, and P. M. Gehring, *Nat. Mater.* **7**, 562 (2008).
- [52] H. Hiraka, S.-H. Lee, P. M. Gehring, G. Xu, and G. Shirane, *Phys. Rev. B* **70**, 184105 (2004).
- [53] Y. Kim, A. S. Disa, T. E. Babakol, and J. D. Brock, *Appl. Phys. Lett.* **96**, 251901 (2010).